Inorganic Chemistry
Article

Inorg. Chem. **2009**, *48*, 10151–10157 **10151**
DOI: 10.1021/ic901172u

Structural Anomalies Associated with Antiferromagnetic Transition of Single-Component Molecular Metal [Au(tmdt)$_2$]

Biao Zhou,[†] Akiko Kobayashi,*[,†] Yoshinori Okano,[‡] HengBo Cui,[§] David Graf,[§] James S. Brooks,[§] Takeshi Nakashima,[∥] Shinobu Aoyagi,[∥] Eiji Nishibori,[∥] Makoto Sakata,[∥] and Hayao Kobayashi*[,†]

[†]*Department of Chemistry, College of Humanities and Sciences, Nihon University, Sakurajosui 3-25-40, Setagaya-Ku, Tokyo 156-8550, Japan,* [‡]*Institute for Molecular Science, Okazaki 444-8585, Japan,* [§]*National High Magnetic Field Laboratory and Physics Department, Florida State University, Tallahassee, Florida 32310, and* [∥]*Department of Applied Physics, Nagoya University, Nagoya 464-8603, Japan*

Received June 18, 2009

The crystal structure of the single-component molecular metal [Au(tmdt)$_2$] was examined by performing powder X-ray diffraction experiments in the temperature range of 9−300 K using a synchrotron radiation source installed at SPring-8. The structural anomalies associated with antiferromagnetic transition were observed around the transition temperature (T_N = 110 K). The continuous temperature dependence of the unit cell volume and the discontinuous change in the thermal expansion coefficient at T_N suggested that the antiferromagnetic transition of [Au(tmdt)$_2$] is a second-order transition. Au(tmdt)$_2$ molecules are closely packed in the (02$\bar{1}$) plane with two-dimensional lattice vectors of *a* and *l* (= 2*a* + *b* + 2*c*). The shortest intermolecular S···S distance along the *a* axis shows a sharp decrease at around T_N, while the temperature dependence of *l* exhibits a characteristic peak in the same temperature region. A distinct structure anomaly was not observed along the direction perpendicular to the (02$\bar{1}$) plane. These results suggest that the molecular arrangement in only the (02$\bar{1}$) plane changes significantly at T_N. Thus, the intermolecular spacing shows anomalous temperature dependence at around T_N only along that direction where the neighboring tmdt ligands have opposite spins in the antiferromagnetic spin structure model recently derived from ab initio band structure calculations. The results of single-crystal four-probe resistance measurements on extremely small crystals (∼25 μm) did not show a distinct resistance anomaly at T_N. The resistance anomaly associated with antiferromagnetic transition, if at all present, is very small. The Au−S bond length decreases sharply at around 110 K; this is consistent with the proposed antiferromagnetic spin distribution model, where the left and right ligands of the same molecule possess opposite spin polarizations. The tendency of the Au−S bond to elongate with decreasing temperature is ascribed to the small energy gap between the *pd*σ(−) (or SOMO + 1) and the *asym-L*π(*d*) (or SOMO) states of the Au(tmdt)$_2$ molecule.

Introduction

[Ni(tmdt)$_2$] is a metallic crystal composed of a single type of molecule (single-component molecular metal), where tmdt (trimethylenetetrathiafulvalenedithiolate) is an extended-TTF-type ligand (TTF = tetrathiafulvalene).[1] The presence of the three-dimensional electron and hole Fermi surfaces in [Ni(tmdt)$_2$] was confirmed experimentally by performing de Haas−van Alphen (dHvA) experiments at very high magnetic fields and low temperatures; this was also theoretically confirmed by ab initio band structure calculations.[2,3] So far, many such single-component molecular metals [M(L)$_2$] have been synthesized, where M = Ni, Pd, Pt, Cu, Au, and Co and L = tmdt, dmdt (dimethyltetrathiafulvalenedithiolate), dt (tetrathiafulvalenedithiolate), and so forth.[1,4] Among these, [Au(tmdt)$_2$], which is isostructural with [Ni(tmdt)$_2$], has gained particular interest. The Au(tmdt)$_2$ molecule ($AuS_{12}C_{18}H_{12}$) has an odd number of total electrons; further, the [Au(tmdt)$_2$]

*To whom correspondence should be addressed: E-mail: akoba@chs.nihon-u.ac.jp.

(1) (a) Tanaka, H.; Okano, Y.; Kobayashi, H.; Suzuki, W.; Kobayashi, A. *Science* **2001**, *291*, 285–287. (b) Kobayashi, A.; Fujiwara, E.; Kobayashi, H. *Chem. Rev.* **2004**, *104*, 5243–5264.

(2) Tanaka, H.; Tokumoto, M.; Ishibashi, S.; Graf, D.; Choi, E. S.; Brooks, J. S.; Yasuzuka, S.; Okano, Y.; Kobayashi, H.; Kobayashi, A. *J. Am. Chem. Soc.* **2004**, *126*, 10518–10519.

(3) Rovira, C.; Novoa, J. J.; Mozos, J. -L.; Ordejon, P.; Canadell, E. *Phys. Rev. B* **2002**, *65*, 081104.

(4) (a) Nunes, J. P. M.; Figueira, M. J.; Belo, D.; Santos, I. C.; Ribeiro, B.; Lopes, E. B.; Henriques, R. T.; Vidal-Gancedo, J.; Veciana, J.; Rovira, C.; Almeida, M. *Chem.—Eur. J.* **2007**, *13*, 9841–9849. (b) Wen, H. -R.; Li, C. -H.; Song, Y.; Zuo, J. -L.; Zhang, B.; You, X. -Z. *Inorg. Chem.* **2007**, *46*, 6837–6839.

(5) (a) Suzuki, W.; Fujiwara, E.; Kobayashi, A.; Fujishiro, Y.; Nishibori, E.; Takata, M.; Sakata, M.; Fujiwara, H.; Kobayashi, H. *J. Am. Chem. Soc.* **2003**, *125*, 1486–1487. (b) Zhou, B.; Shimamura, M.; Fujiwara, E.; Kobayashi, A.; Higashi, T.; Nishibori, E.; Sakata, M.; Cui, H.; Takahashi, K.; Kobayashi, H. *J. Am. Chem. Soc.* **2006**, *128*, 3872–3873.

Published on Web 09/25/2009

crystal undergoes antiferromagnetic transition at 110 K ($= T_N$), while maintaining a metallic state at lower temperatures.[5,6] This magnetic transition temperature is extremely high as compared to the transition temperatures of common magnetic organic metals consisting of organic π donors and inorganic anions, such as the ferromagnetic organic metal (BEDT-TTF)$_3$[MCr(C_2O_4)$_3$](CH_2Cl_2) (BEDT-TTF = bis(ethylenedithio)tetrathiafulvalene; T_c = 5.5 K (M = Mn), 9.2 K (M = Co))[7,8] and the antiferromagnetic organic superconductor κ-$BETS_2FeBr_4$ (BETS = bis(ethylendithio)tetraselenafulvalene; T_N = 2.5 K and T_c = 1.1 K);[9,10] however, the magnetic transition temperature of [Au(tmdt)$_2$] is comparable to that of the typical inorganic antiferromagnetic metal Mn ($T_N \approx$ 100 K). The three-dimensionality of the electronic structure of [Au(tmdt)$_2$] is considered as the main factor responsible for the high magnetic transition temperature.[6,11] We performed X-ray diffraction experiments on [Au(tmdt)$_2$] at various temperatures to identify the possible structural anomalies associated with its antiferromagnetic transition. In this paper, we report the temperature dependence of the crystal structure of [Au(tmdt)$_2$]. The results of four-probe resistivity measurements are also briefly discussed.

Experimental Section

[Au(tmdt)$_2$] crystals were prepared electrochemically using standard H-type cells. All synthesis procedures were carried out in a strictly inert atmosphere using the Schlenk technique. The starting material (^{n}Bu$_4$N)[Au(tmdt)$_2$] was prepared according to the previously reported procedure with certain modifications.[1b] Thin-plate microcrystals were grown on a Pt electrode over approximately 4 weeks. X-ray powder analyses of the crystal structure of [Au(tmdt)$_2$] were carried out using microcrystals with dimensions of approximately 20 μm, which is suitable for X-ray powder diffraction experiments. In addition, single-crystal X-ray structure measurements were carried out at 270 K, 180 K, and 80 K using a thin-plate crystal with a size of approximately 50 μm; these measurements were carried out on a Rigaku AFC-8 Mercury CCD diffractometer with graphite monochromated Mo Kα radiation (λ = 0.7107 Å) and a confocal X-ray mirror. Although the reliability factors were not significantly high (R = 0.058 (270 K), 0.056 (180 K), and 0.070 (80 K)), the accuracy of lattice constants was considerably lower than that determined by the powder method. Therefore, we do not include the results of single-crystal diffraction studies in the present paper, except those on the Au−S bond lengths. The powder X-ray diffraction experiments were performed at the SPring-8 facility at the beamline BL02B2. The experiments using the Debye−Scherrer camera were performed at 90 K, 130 K, 200 K, and 300 K with the wavelength of the incident X-ray as 1.0474 Å; the experiments using the plate-type camera were performed at 9 K, 30 K, 55 K, 79 K, 104 K, 114 K, and 124 K with the wavelength of the incident X-ray as 0.50247 Å. The lattice constants obtained at 300 and 9 K are as follows: at 300 K, a = 6.40300(3) Å, b = 7.48728(5), c = 12.13352(6), α = 90.2313(4)°, β = 96.6760(3), γ = 103.1443(5), and V = 562.333(7) Å^3; at 9 K, a = 6.35584(5) Å, b = 7.35278(5), c = 12.08905(8), α = 89.7445(9)°, β = 96.4578(7), γ = 103.0535(9), and V = 546.74(1) Å^3. The structure was refined by the MEM/Rietveld method. The R-factors were as follows: 0.0239 (9 K), 0.0233 (30 K), 0.0239 (55 K), 0.0242 (79 K), 0.0266 (90 K), 0.0241 (104 K), 0.0249 (114 K), 0.0247 (124 K), 0.0229 (130 K), 0.0272 (200 K), and 0.0323 (300 K).

Four-probe resistance measurements were successfully performed using very small thin single crystals with a size of approximately 25 μm. Four gold wires with a diameter of 5 μm were manually bonded to the microcrystal using gold paint and were used as leads.

Results and Discussion

[Au(tmdt)$_2$] exhibits distinct bulk electromagnetic properties such as those described in previous papers.[5,6] Using crystals with dimensions of approximately 20 μm, X-ray powder analyses were carried out at a temperature range of 9−300 K. As previously reported,[5] the [Au(tmdt)$_2$] crystal belongs to a triclinic system with the space group $P\bar{1}$. The temperature (T) dependences of unit cell volume (V) and lattice constants of this crystal are shown in Figure 1a,b. The thermal expansion coefficient ($\alpha = (dV/dT)/V$) at room temperature is found to be 1.2×10^{-4} (K^{-1}). This value is approximately three times that of gold (0.4×10^{-4}) and half that of anthracene (2.0×10^{-4}). Considering the fact that a single-component molecular metal simultaneously exhibits the properties of both a metallic crystal and a molecular crystal,[12] it is expected that the thermal expansion coefficient of [Au(tmdt)$_2$] naturally takes an intermediate value between that of typical metallic crystal and that of typical molecular crystal. As shown in Figure 1a, an anomaly is observed in the $T-V$ curve, indicating the occurrence of a second-order phase transition at around 110 K; at this temperature, the thermal expansion coefficient shows a discontinuous change. This transition temperature is in good agreement with the reported antiferromagnetic transition temperature. Therefore, the magnetic transition of [Au(tmdt)$_2$] is a second-order transition. Figure 1b shows the temperature dependences of the magnitudes of the thermal contractions of the lattice constants, that is, Δa, $\Delta b/2$, and Δc; $\Delta b/2$ is plotted instead of Δb because in contrast to the a and c directions, along which uniform molecular arrangements are observed, along the b direction, two molecules exist in each period (see Figure 1c, d). Similar to the temperature dependence of V, the temperature dependences of Δa, $\Delta b/2$, and Δc show anomalies at around 110 K. However, the anomalies in the case of Δa and Δc are clearly observed, while no distinct anomaly is observed in the case of $\Delta b/2$. As reported earlier, all the Au(tmdt)$_2$ molecules are located on the lattice points, and one-half of the molecule, located on (0, 0, 0), is crystallographically independent (in this paper, Au(tmdt)$_2$ without brackets is used to represent the molecule and [Au(tmdt)$_2$] is used to represent the crystal).[5] Along the a direction, there are many intermolecular S···S contacts, with distances shorter than the van der Waals distance (r_{vdW}(S···S) = 3.70 Å). At 300 K, S2(x, y, z)···S1(1 + x, y, z), 3.313 Å; S1(−x, −y, −z)···S1-(1 + x, y, z), 3.344 Å; S2(x, y, z)···S3(1 + x, y, z), 3.408 Å; S4(x, y, z)···S3(1 + x, y, z), 3.628 Å; S4(x, y, z)···S5(1 + x,

(6) Hara, Y.; Miyagawa, K.; Kanoda, K.; Shimamura, M.; Zhou, B.; Kobayashi, A.; Kobayashi, H. *J. Phys. Soc. Jpn.* **2008**, *77*, 053706.
(7) Coronado, E.; Galán-Mascarós, J. R.; Gómez-Garcia, C. J.; Laukhin, V. *Nature* **2000**, *408*, 447–449.
(8) Coronado, E.; Day, P. *Chem. Rev.* **2004**, *104*, 5419–5448.
(9) Ojima, E.; Fujiwara, H.; Kato, K.; Kobayashi, H.; Tanaka, H.; Kobayashi, A.; Tokumoto, M.; Cassoux, P. *J. Am. Chem. Soc.* **1999**, *121*, 5581–5582.
(10) Kobayashi, H.; Cui, H.; Kobayashi, A. *Chem. Rev.* **2004**, *104*, 5265–5288.
(11) Seo, H.; Ishibashi, S.; Okano, Y.; Kobayashi, H.; Kobayashi, A.; Fukuyama, H.; Terakura, K. *J. Phys. Soc. Jpn.* **2008**, *77*, 023714.
(12) Okano, Y.; Zhou, B.; Tanaka, H.; Adachi, T.; Ohishi, Y.; Takata, M.; Aoyagi, S.; Nishibori, E.; Sakata, M.; Kobayashi, A.; Kobayashi, H. *J. Am. Chem. Soc.* **2009**, *131*, 7169–7174.

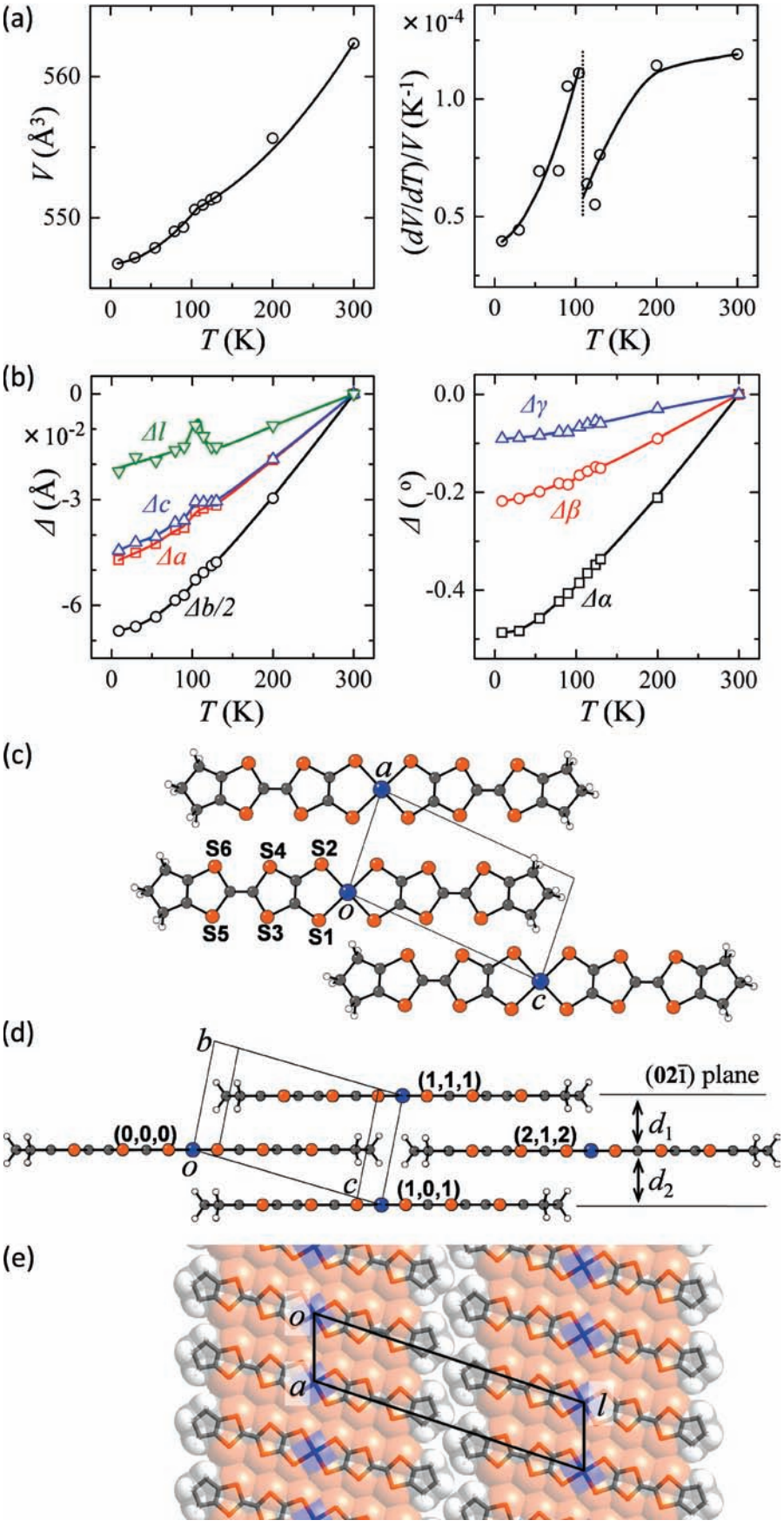

Figure 1. (a) Temperature dependences of unit cell volume and thermal expansion coefficient ($(dV/dT)/V$). (b) Changes in lattice constants with varying temperature. The lattice constants at 9 and 300 K are given in the Experimental Section. (c) Molecular arrangement in the *ac* plane. (d) Mode of molecular stacking along the *b* direction. The interplanar distances are $d_1 = 3.540$ Å (300 K), 3.457 (9 K) and $d_2 = 3.629$ (300 K), 3.571 (9 K). (e) Mode of molecular packing in (02$\bar{1}$) plane. The change in l ($= |2a + b + 2c|$) with temperature is also shown.

y, z), 3.650 Å; S6(x, y, z)···S5($1 + x, y, z$), 3.625 Å, where Sj(x, y, z) is the jth S atom on (0, 0, 0) (Figure 1c). In contrast, along the c direction, S···S contacts shorter than r_{vdW}-(S···S) do not exist between the molecules (between the molecules located on (0, 0, 0) and (0, 0, 1)); at 300 K, the shortest distance of 3.734 Å (S2($-x, -y, -z$)···S6($x, y, 1 + z$)) is slightly greater than r_{vdW}(S···S). Along the b direction, the right half of the molecule on (0, 0, 0) overlaps with the left halves of the molecules on (1, 0, 1) and (1, 1, 1) (Figure 1d). The shortest intermolecular S···S distance between these molecules (3.804 Å at 300 K) is fairly greater than r_{vdW}-(S···S). The large thermal contraction along the b direction is consistent with the weak intermolecular contacts observed along this direction (Figure 1b).

As shown in Figure 1c,e, Au(tmdt)$_2$ molecules are arranged side-by-side along the a axis to form "molecular tapes". As a result of the presence of peripheral trimethylene groups, the molecular tape has a sawtooth-like structure, and the neighboring tapes are closely interlocked with each other to form a metal layer, similar to a graphite sheet, parallel to the (02$\bar{1}$) plane (Figure 1d); a and l ($= 2a + b + 2c$) are the lattice vectors (Figure 1e). Since the van der Waals interaction between S atoms is considered to be much stronger than that between methylene groups, the intermolecular contact along a was expected to be considerably shorter than that along l. In addition, the strong intermolecular S···S contact along the a axis is considered to stabilize the metal band. Nevertheless, the temperature dependence of l is found to be lower than that of a, indicating a very tight packing of molecular tapes. In addition, the temperature dependence curve of Δl exhibits a characteristic peak at around 110 K (Figure 1b). Considering that the molecular structure, except at the terminal trimethylene groups, is rigid, this anomalous peak is ascribed to the positional freedom of the trimethylene groups. However, clear evidence for the conformational change of trimethylene groups at around 110 K were not obtained from our results; this is because the magnitude of the anomaly (~0.005 Å) was considerably smaller than the standard deviation of the C−C bond length (0.02−0.03 Å). The anomalous peak in the Δl vs T curve suggests that the antiferromagnetic transition of [Au(tmdt)$_2$] is accompanied with a characteristic deformation of the molecular sheet.

Temperature dependences of the shortest intermolecular S···S distance along the a and c axes are shown in Figure 2a. The shortest intermolecular S···S distance along the a direction (S2(x, y, z)···S1($1 + x, y, z$)) exhibits a sharp decrease around T_N (see also Figure 1c). In contrast, the shortest intermolecular S···S distance along the c axis (S2($-x, -y, -z$)···S6($x, y, 1 + z$)) does not exhibit a distinct anomaly around T_N. The temperature dependences of the short intermolecular S···S distances along the b direction (S3($-x, -y, -z$)···S5($1 + x, y, 1 + z$) and S3($-x, -y, -z$)···S6($1 + x, 1 + y, 1 + z$)) are also shown; however, these distances are greater than the van der Waals distance (3.70 Å). These curves show a monotonous decrease with temperature (Figure 2b). The anomalies observed at T_N in the temperature dependences of a, l, and the S···S contacts along a and the subtle anomalies in the temperature dependence of b and the S···S contact along c and b suggest that the molecular arrangement of only the (02$\bar{1}$) plane changes significantly at T_N. These results appear to be consistent with the antiferromagnetic spin structure model derived from the results of the ab initio band calculations; in these calculations,

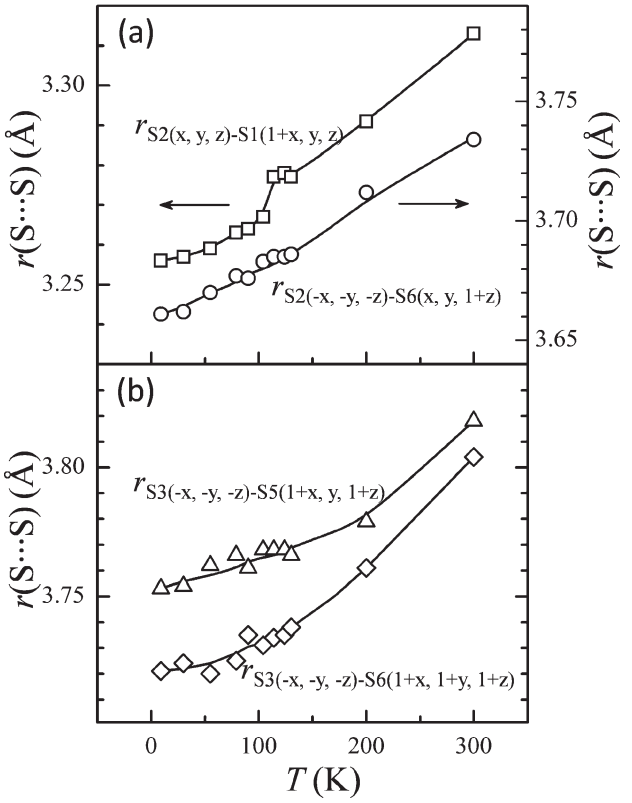

Figure 2. (a) Temperature dependences of shortest intermolecular S···S distances along the a and c directions (see Figure 1c). (b) Temperature dependences of intermolecular short S···S distances along the b axis (see Figure 1c,d).

the spins on each tmdt ligand were assumed to exhibit antiferromagnetic distribution along the a and l directions and ferromagnetic distribution along the b direction (Figure 3).[13] From the above results, it is apparent that significant structural anomaly is observed along only those directions in which alternate up and down spin polarizations develop on the neighboring tmdt ligands below T_N.

It was reported that the temperature dependence of the resistivity of [Au(tmdt)$_2$], measured using compact pellets of crystalline powder, showed a nonmetallic behavior at room temperature despite the high conductivity (~50 S cm^{-1}).[5b] In addition, no anomaly in resistivity was observed at T_N. The four-probe resistivity measurements could not be performed on [Au(tmdt)$_2$] crystals because of their small size; however, Tanaka et al. performed two-probe resistance measurements on microcrystals grown on finely patterned interdigitated electrodes; their results suggested that [Au(tmdt)$_2$] was metallic even at temperatures as low as liquid helium temperature, as expected.[14] In this experiment, however, a clear anomaly was not observed around T_N. Because the results of ab initio band calculations suggest that the nesting of Fermi surfaces occurs at T_N,[13] it is highly probable that a possible resistance anomaly is observed at the magnetic transition temperature by performing four-probe single crystal resistance measurements. Recently, we succeeded in bonding four gold wires with the diameters of 5 μm by

(13) Ishibashi, S.; Tanaka, H.; Kohyama, M.; Tokumoto, M.; Kobayashi, A.; Kobayashi, H.; Terakura, K. *J. Phys. Soc. Jpn.* **2005**, *74*, 843–846.
(14) Tanaka, H.; Hara, S.; Tokumoto, M.; Kobayashi, A.; Kobayashi, H. *Chem. Lett.* **2007**, *36*, 1006–1007.

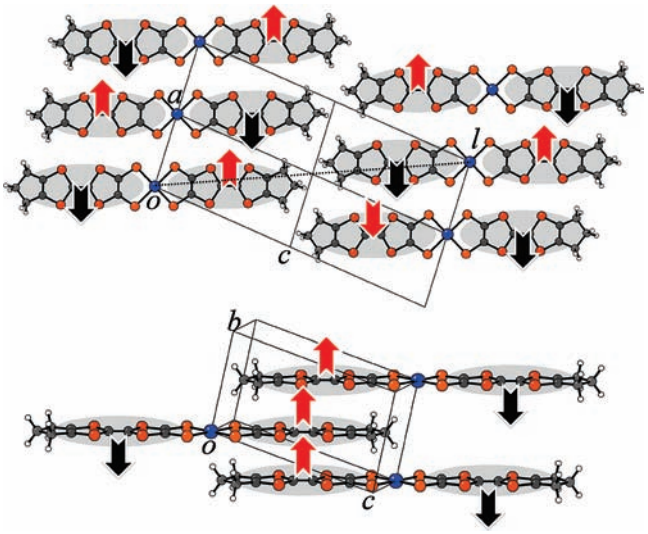

Figure 3. Antiferromagnetic spin structure model derived from ab initio electronic band structure calculations.[13] The arrows indicate up and down spin distributions.

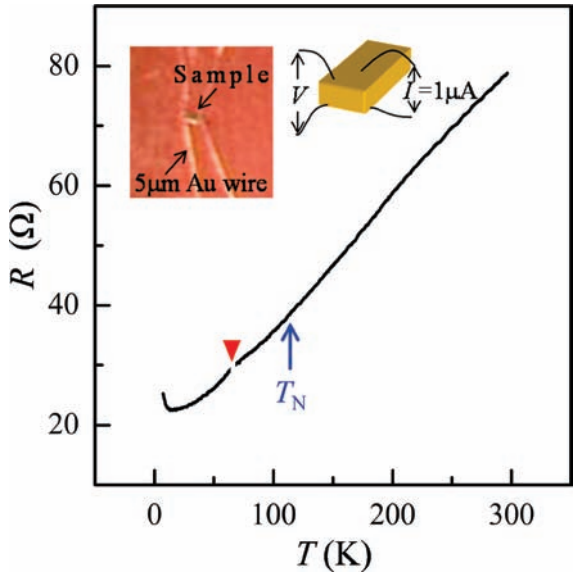

Figure 4. Temperature dependence of resistance of single crystal of $[Au(tmdt)_2]$. An inverted triangle indicates the temperature at which a small resistance jump probably due to a crack in the crystal was observed.

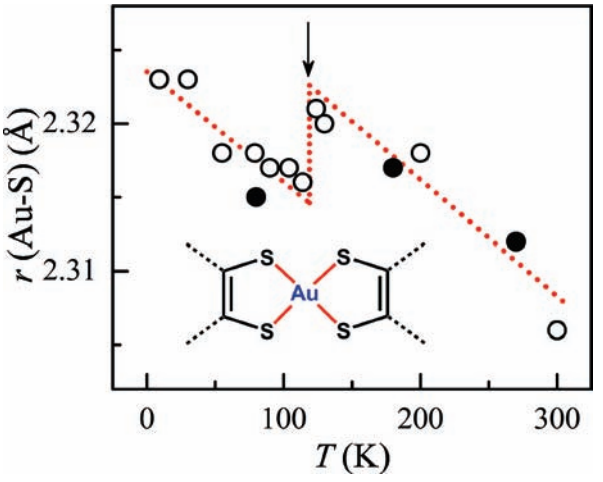

Figure 5. Temperature dependence of Au−S bond length determined by powder X-ray structure determination. The solid circles indicate the bond lengths determined by single-crystal structure analyses. The standard deviation of Au−S bond length is 0.002−0.003 Å for the powder structure analyses and 0.001 Å for single-crystal structure analyses.

manually applying gold paint to the extremely brittle thin-plate microcrystals with maximum dimensions of less than 25 μm and carried out four-probe resistance measurements at low temperatures. The resistance (R) decreased continuously with decreasing temperature (T) (Figure 4). A decrease in resistance at low temperatures was also observed in another crystal, although accurate resistance measurement could not be performed due to a problem encountered in one of the four terminals. Except for a slight bending of the $R-T$ curve at around 110 K, no resistance anomaly was observed. A small increase in resistance was observed in the low temperature region; however, at present, it is not clear whether this increase in resistance is intrinsic or caused by external factors, which is because the resistance behavior at low temperatures is not very reliable owing to a resistance jump at 66 K. Nonetheless, the existence of the metallic state below T_N was confirmed for the first time from single-crystal resistance measurement results. These results also confirm that the resistance anomaly at T_N, if at all present, is small. Further experiments are required to elucidate the precise resistance behavior of the metal below T_N.

An unpaired electron of an isolated $Au(tmdt)_2$ molecule occupies a SOMO (singly occupied molecular orbital) and participates in the formation of a conduction band. In the case of an antiferromagnetic phase of a system, which consists of planar π molecules with unpaired electrons, it is usually considered that the molecules with up spins and those with down spins are arranged alternately. However, as mentioned before, a characteristic antiferromagnetic spin structure for the antiferromagnetic phase of $[Au(tmdt)_2]$ has been proposed on the basis of the ab initio band structure calculations (Figure 3):[13] the up and down spins are distributed independently on the left and right tmdt ligands of one $Au(tmdt)_2$ molecule.

As shown in Figure 5, at around T_N, the Au−S bond length decreases by approximately 0.007 Å. In the case of an isostructural $Ni(tmdt)_2$ molecule, it was reported that the Ni−S bond length decreases by approximately 0.026 Å during the electrochemical oxidation of the molecule ($[Ni(tmdt)_2]^{2-} \rightarrow [Ni(tmdt)_2]^0$).[1,15,16] In other words, on oxidation, two electrons from the highest occupied orbital of the dianionic $Ni(tmdt)_2$ molecule are lost; this orbital essentially corresponds to the SOMO of $Au(tmdt)_2$. Since this molecular orbital has an antibonding character with respect to the Ni−S bond, it is expected that the Ni−S bond length would decrease on the oxidation of $[Ni(tmdt)_2]^{2-}$. In the expected spin structure model of $[Au(tmdt)_2]$, the left and right ligands of the same molecule have opposite spin distributions (Figure 3). To achieve this spin distribution, the spin density on the central Au atom must be zero because the Au atom cannot simultaneously possess up and down spins. Consequently, at T_N, the antibonding character of the

(15) Tanaka, H.; Kobayashi, H.; Kobayashi, A. *J. Am. Chem. Soc.* **2002**, *124*, 10002–10003.

(16) Kobayashi, A.; Okano, Y.; Kobayashi, H. *J. Phys. Soc. Jpn.* **2006**, *75*, 051002.

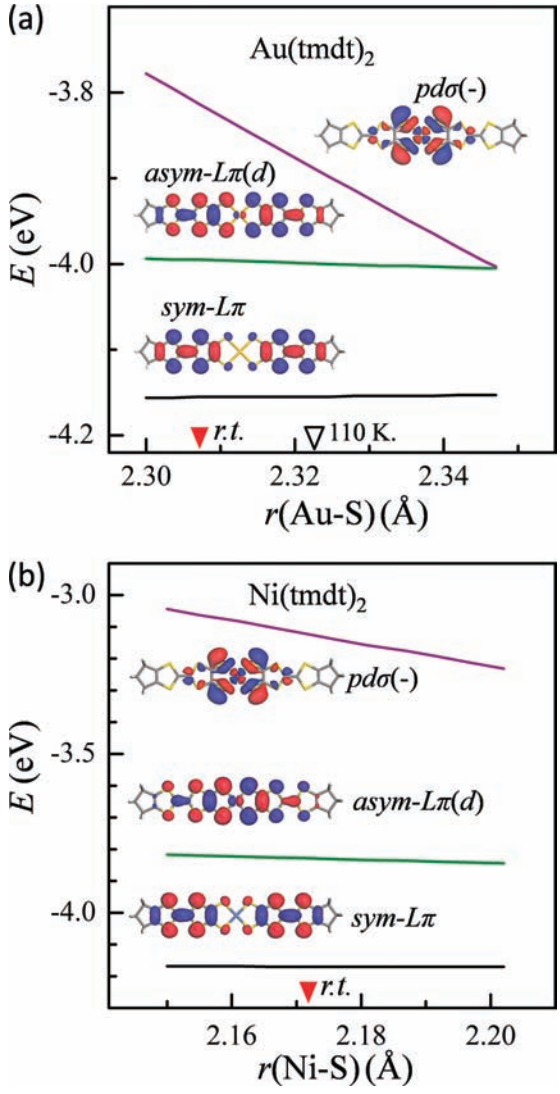

Figure 6. Dependences of energies of $pd\sigma(-)$, *sym-Lπ*, and *asym-Lπ*(*d*) states on M−S (M = Au, Ni) bond length: (a) $Au(tmdt)_2$, (b) $Ni(tmdt)_2$. The inverted red and white triangles correspond to the M−S bond lengths at room temperature (M = Au, Ni) and at 110 K (M = Au), respectively.

Au−S bond contributed from the SOMO must have weakened, resulting in a decrease in the Au−S bond length. In the case of electrocrystallization of $[Ni(tmdt)_2]^{2-}$, the extent of the decrease in the Ni−S bond length is 0.013 Å per one-electron oxidation. The relatively small change in Au−S bond length (0.007 Å) is consistent with the fact that the *d* component of the SOMO of the $Au(tmdt)_2$ molecule is small (see Figure 6).[17] Thus, the sharp decrease in Au−S bond length at around T_N can be regarded as structural evidence for the antiferromagnetic spin polarization occurring within one molecule. The S−Au−S bond angles of $Au(tmdt)_2$ molecule seem to show a sharp increase around T_N; however, the deviation of the data is too large to discuss in detail.

Besides the sharp decrease in Au−S bond length at T_N, it is conspicuous that the Au−S bond length (r(Au−S)) tends to increase with decreasing temperature. The magnitude of the change in the Au−S bond length as temperature decreases from 300 to 110 K is approximately 0.014 Å, which is considerably higher than the standard deviation of the Au−S bond length (σ(Au−S) = 0.002 Å). It is interesting to determine whether a similar increase in the M−S bond length is observed in the isostructural $[M(tmdt)_2]$ (M = Ni, Pt). In the case of $[Pt(tmdt)_2]$, whose crystal structures were determined by powder X-ray diffraction experiments, no significant change was observed in the bond length: r(Pt−S) = 2.299(5) Å at 300 K and 2.299(5) Å at 130 K.[18,19] In the case of $[Ni(tmdt)_2]$, the Ni−S distance was determined to be 2.171(4) Å at 300 K by X-ray powder diffraction analysis[19] and 2.177(1) Å at 123 K by single-crystal X-ray structure analysis.[1a] Thus, no significant change in the M−S bond length (r(M−S)) with temperature was observed in $[Pt(tmdt)_2]$ or $[Ni(tmdt)_2]$. On the basis of the ab initio electronic band structure calculations, Ishibashi pointed out that the small energy difference between SOMO and SOMO + 1 (or LUMO) states is a remarkable feature of the electronic structure of $[Au(tmdt)_2]$.[17] In accordance with ref 17, where the SOMO + 1 state is referred to as the $pd\sigma(-)$ state, we shall hereafter refer to the SOMO state as *asym-Lπ*(*d*), because this molecular orbital possesses the antisymmetric combination of the π orbitals of the left and right ligands and a small contribution of *d* orbital of the central transition-metal atom (see Figure 6). Similarly, the SOMO − 1 orbital without the contribution of the *d* orbital is referred to as the *sym-Lπ* because the molecular orbital possesses a symmetric combination of the π orbitals of the left and right ligands.[13,20] According to this representation of molecular orbitals, the HOMO and LUMO of $M(tmdt)_2$ molecule (M = Ni, Pt) can be referred to as *sym-Lπ* and *asym-Lπ*(*d*), respectively. Recently, Seo pointed out that the important molecular orbitals near the Fermi level can be reconstructed by the combination of three virtual molecular orbitals within the molecule.[11] To clarify the consistency between the present representation and Seo's concept of reconstruction of frontier orbitals, a slight modification of the *composite orbitals* would be required. However, in this paper, we tentatively adopt the above-mentioned representation (*sym-Lπ*, *asym-Lπ*(*d*), and $pd\sigma(-)$). We performed GGA-DFT (generalized gradient approximation-density functional theory) calculations using DMol[3] code[21,22] to obtain the r(M−S) dependence of the energy levels of *sym-Lπ*, *asym-Lπ*(*d*), and $pd\sigma(-)$ states of $[M(tmdt)_2]$ (M = Au, Ni, Pt). As shown in Figure 6, the energy level of $pd\sigma(-)$ shows a strong decrease with increasing r(M−S). The energy level of *asym-Lπ* shows a weak dependence on r(M−S), while that of *sym-Lπ*(*d*) is almost independent of r(M−S). Considering the difference between the bonding (or nonbonding) character of these orbitals on the M−S bond, these results are reasonable. As mentioned

(17) Ishibashi, S.; Terakura, K.; Kobayashi, A. *J. Phys. Soc. Jpn.* **2008**, *77*, 024702.

(18) Zhou, B.; Kobayashi, A.; Okano, Y.; Nakashima, T.; Aoyagi, S.; Nishibori, E.; Sakata, M.; Tokumoto, M.; Kobayashi, H. *Adv. Mater.* **2009**, *21*, 3596−3600.

(19) Nakashima, T. Low temperature structure analyses of single-component molecular metals based on synchrotron radiation X-ray diffraction experiments. Master Thesis (in Japanese), Nagoya University, 2007.

(20) Kobayashi, A.; Tanaka, H.; Kobayashi, H. *J. Mater. Chem.* **2001**, *11*, 2078–2088.

(21) (a) Delley, B. *J. Chem. Phys.* **1990**, *92*, 508–517. (b) Delley, B. *J. Chem. Phys.* **2000**, *113*, 7756–7764 (DMol[3] is available as part of Material Studio).

(22) Perdew, J. P.; Burke, K.; Ernzerhof, M. *Phys. Rev. Lett.* **1996**, *77*, 3865–3868.

above, the $pd\sigma(-)$ orbital has antibonding (on M−S bond) and σ-type character. Consequently, the energy of the $pd\sigma(-)$ state ($\varepsilon(pd\sigma(-))$ drastically decreases with an increase in r(M−S): $d\varepsilon(pd\sigma(-))/dr$(Au−S) = −4.80 eV/Å for $Au(tmdt)_2$) and −3.59 eV/Å for $Ni(tmdt)_2$. Similarly, the energy of the *asym-L*$\pi(d)$ state decreases with increasing r(M−S) due to the antibonding combination of $d\pi$(M) and $p\pi$(S) orbitals. However, the dependence of orbital energy on bond length is much weaker because of the relatively small amplitude of the d orbital and π character of *asym-L*$\pi(d)$: $d\varepsilon(asym\text{-}L\pi(d))/dr$(M−S) = −0.24 eV/Å for $Au(tmdt)_2$ and −0.52 eV/Å for $Ni(tmdt)_2$. The $d\varepsilon(asym\text{-}L\pi(d))/dr$(M−S) value of $Ni(tmdt)_2$ is approximately twice that of $Au(tmdt)_2$, which is consistent with the fact that $Ni(tmdt)_2$ has a larger d component, as mentioned before[17] (Figure 6a,b). Further, a smaller $d\varepsilon(asym\text{-}L\pi(d))/dr$(M−S) value of $Au(tmdt)_2$ is consistent with the small discontinuous decrease in r(Au−S) at T_N. Finally, $\varepsilon(sym\text{-}L\pi)$ is almost independent of r(M−S) because of the zero amplitude of the molecular orbital on M.

As pointed out by Isibashi,[17] the energy difference between $pd\sigma(-)$ and *asym-L*$\pi(d)$ states (Δ) of $Au(tmdt)_2$ is much smaller than that in the case of $Ni(tmdt)_2$. The Δ value calculated using the molecular structure determined at room temperature is 0.18 eV for $Au(tmdt)_2$ and 0.71 eV for $Ni(tmdt)_2$. Similar calculations performed on $Pt(tmdt)_2$ gave the Δ value of 1.2 eV (r(Pt−S) = 2.291 Å at room temperature).[18] When the energy level of the vacant $pd\sigma(-)$ state approaches the energy level of the singly occupied *asym-L*$\pi(d)$ state, the energy of the *asym-L*$\pi(d)$ state is suppressed by the intermolecular interaction between $pd\sigma(-)$ and *asym-L*$\pi(d)$ orbitals. Thus, it is evident that the electronic energy of $[Au(tmdt)_2]$ decreases with increasing Au−S bond length. This may be the main reason why the Au−S bond length tends to increase with decreasing temperature, except at the temperature around T_N. The intermolecular $pd\sigma(-)$-*asym-L*$\pi(d)$ interaction will be less crucial in $Ni(tmdt)_2$ and $Pt(tmdt)_2$ because Δ is considerably higher than this interaction (< 0.1 eV).[11] As mentioned above, a clear temperature dependence of r(M−S) has not been observed in the case of $[M(tmdt)_2]$ (M = Ni, Pt); this result is consistent with the large Δ values of $Ni(tmdt)_2$ and $Pt(tmdt)_2$.

Conclusion

The X-ray powder diffraction experiments were performed on the single-component molecular metal $[Au(tmdt)_2]$ at 9−300 K using synchrotron radiation. The temperature dependence of the unit cell volume revealed that the antiferromagnetic transition of $[Au(tmdt)_2]$ at 110 K is a second-order transition. The $Au(tmdt)_2$ molecules are closely packed in the $(02\bar{1})$ plane whose two-dimensional lattice vectors are a and l ($= 2a + b + 2c$). The temperature dependences of a, l, and the shortest intermolecular S···S distance along a showed anomalies at T_N; however, such a distinct anomaly was not observed along the b direction. The results of single-crystal four-probe resistance measurements, which were performed using extremely small crystals (∼25 μm), did not show a distinct resistance anomaly at T_N. Although precise resistance measurements must be further conducted to elucidate the detailed resistance behavior around T_N, the resistance anomaly associated with antiferromagnetic transition, if present, is found to be small. The Au−S bond length sharply decreases at around 110 K; this result is consistent with the antiferromagnetic spin polarization in the $Au(tmdt)_2$ molecule below T_N, as previously reported on the basis of ab initio electronic band structure calculations. The tendency of the Au−S bond to increase with decreasing temperature may be ascribed to the small energy difference between the $pd\sigma(-)$ and *asym-L*$\pi(d)$ states of the $Au(tmdt)_2$ molecule.

Acknowledgment. This study was financially supported by a Grant-in-Aid for Scientific Research (B) (No. 20350069) and Innovative Areas (20110003) of Ministry of Education, Culture, Sports, Science and Technology of Japan. The study was also supported by "Strategic Research Base Development" Program for Private Universities subsidized by MEXT (2009) (S0901022). The synchrotron radiation experiments were performed at the BL02B2 installed at the facility SPring-8 with the approval of the Japan Synchrotron Radiation Research Institute (JASRI). We thank Mr. M. Maeyama of Rigaku Corporation for single-crystal X-ray data collections.

Supporting Information Available: X-ray crystallographic files in CIF format. This material is available free of charge via the Internet at http://pubs.acs.org.